

See discussions, stats, and author profiles for this publication at: <https://www.researchgate.net/publication/232717526>

# Nano-Fe-O Encapsulated in Microcarbon Spheres: Synthesis, Characterization, and Environmental Applications

ARTICLE in ACS APPLIED MATERIALS & INTERFACES · OCTOBER 2012

Impact Factor: 6.72 · DOI: 10.1021/am301829u · Source: PubMed

---

CITATIONS

37

READS

291

## 6 AUTHORS, INCLUDING:



Guanliang Zhou

Curtin University

8 PUBLICATIONS 191 CITATIONS

[SEE PROFILE](#)



Ha Ming Ang

Curtin University

102 PUBLICATIONS 1,964 CITATIONS

[SEE PROFILE](#)



Moses O. Tadé

Curtin University

348 PUBLICATIONS 4,175 CITATIONS

[SEE PROFILE](#)



Shaobin Wang

Curtin University

271 PUBLICATIONS 9,327 CITATIONS

[SEE PROFILE](#)

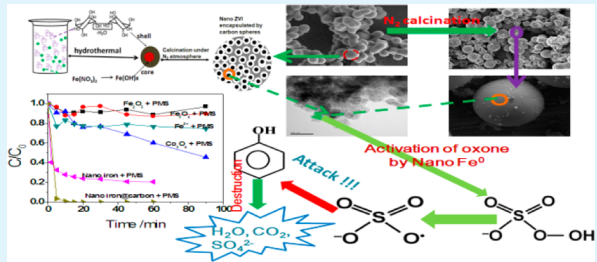
# Nano-Fe<sup>0</sup> Encapsulated in Microcarbon Spheres: Synthesis, Characterization, and Environmental Applications

Hongqi Sun,\* Guanliang Zhou, Shizhen Liu, Ha Ming Ang, Moses O Tadé, and Shaobin Wang\*

Department of Chemical Engineering and CRC for Contamination Assessment and Remediation of the Environment (CRC-CARE), Curtin University, GPO Box U1987, WA 6845, Australia

Supporting Information

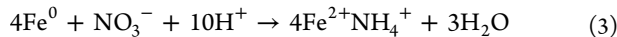
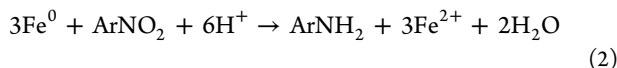
**ABSTRACT:** Nanoscaled zerovalent iron (ZVI) encapsulated in carbon spheres (nano-Fe<sup>0</sup>@CS) were prepared via a hydrothermal carbonization method, using glucose and iron(III) nitrate as precursors. The properties of the nano-Fe<sup>0</sup>@CS were investigated by X-ray diffraction (XRD), thermogravimetric analysis-differential scanning calorimetry (TGA-DSC), Fourier transform infrared spectroscopy (FTIR), scanning electron microscopy (SEM), transmission electron microscopy (TEM), and nitrogen adsorption/desorption isotherms. Nano-Fe<sup>0</sup>@CS was demonstrated, for the first time, as an effective material in activating Oxone (peroxymonosulfate, PMS) for the oxidation of organic pollutants. It was found that the efficiency of nano-Fe<sup>0</sup>@CS was higher than ZVI particles, iron ions, iron oxides, and a cobalt oxide. The mechanism of the high performance was discussed. The structure of the nano-Fe<sup>0</sup>@CS not only leads to high efficiency in the activation of PMS, but also good stability. This study extended the application of ZVI from reductive destruction of organics to oxidative degradation of organics by providing a green material for environmental remediation.



**KEYWORDS:** zerovalent iron, peroxymonosulfate, carbon nanosphere, phenol, nanoparticles, chemical oxidation

## 1. INTRODUCTION

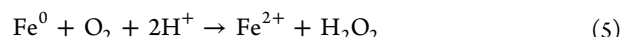
Iron is a low-cost, naturally abundant, and environmentally friendly material that has been widely applied in remediation of various contaminants in water<sup>1,2</sup> or soil.<sup>3</sup> There were extensive studies of zerovalent iron (ZVI) for use in the decontamination of halogenated organics,<sup>3,4</sup> as well as applications as nitro aromatic compounds,<sup>5</sup> dyes,<sup>6</sup> pesticides,<sup>7</sup> nitrates,<sup>1</sup> and heavy metals.<sup>8,9</sup> In these applications, ZVI was exclusively used as a strong reductant, and relative reactions can be described as shown below.<sup>1,5,10</sup>



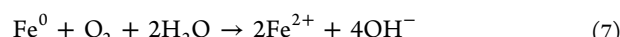
However, the reduction performance of ZVI fails to facilitate the degradations of those organics that cannot directly receive electrons, such as phenol.<sup>11,12</sup> To overcome the barrier of contaminant dependence, it is highly desirable to develop oxidation reactions using ZVI.<sup>13</sup>

Compared to the extensive investigations of reactive reduction, only a few oxidations of organic pollutants using ZVI have been conducted. The oxidation was generally initiated by the reactivity of ZVI with dissolved oxygen,<sup>13,14</sup> hydrogen

peroxide,<sup>15–17</sup> or persulfate.<sup>18–22</sup> The former two oxidations proceed in the following mechanism.<sup>14</sup>



The activation of persulfate (peroxydisulfate, PDS) for oxidation of organic pollutants can be obtained via the following reactions:<sup>19,21,22</sup>



To the best of our knowledge, there is no study using ZVI to activate peroxymonosulfate (PMS, commercially known as Oxone;  $2\text{KHSO}_5 \cdot \text{KHSO}_4 \cdot \text{K}_2\text{SO}_4$ ), although a ferrous PMS system has been reported.<sup>23</sup>

Recently, it was found that nanoscale ZVI can show a higher activity in reduction reactions, when compared to conventional microscale ZVI particles.<sup>1,4,10</sup> Nanoscaled Fe<sup>0</sup> generally offers high surface-area-to-volume ratios, high specific surface area, and high surface reactivity. But it favors strong aggregation into microscale particles, because of high surface energy and intrinsic magnetic interaction.<sup>24</sup> Thus, many materials have

Received: August 30, 2012

Accepted: October 29, 2012

Published: October 29, 2012



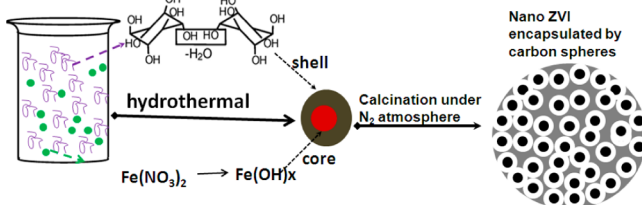
been employed as supports for nano- $\text{Fe}^0$  for a better Fe distribution, including polystyrene resin,<sup>25</sup> alumina,<sup>26</sup> bentonite,<sup>27</sup> kaolinite,<sup>28</sup> zeolite,<sup>29</sup> carbon black,<sup>30</sup> activated carbon,<sup>31</sup> carbon nanotubes,<sup>32</sup> and carbon spheres.<sup>33</sup> Most of supported Fe<sup>0</sup> was prepared by a liquid-phase reduction method using borohydride salt.<sup>25–29,31,32</sup> However, the N<sub>2</sub> atmosphere, vacuum operation, high cost of borohydride, and the production of large volume of hydrogen make such a process complex and cost-intensive. Furthermore, without calcination, the mechanical stability of nano-Fe<sup>0</sup> on supports would be an additional issue that might influence the dispersion and mechanical strength of ZVI. Hoch et al.<sup>30</sup> reported that ZVI nanoparticles could be prepared by the reduction of carbon black, which was also used as a support material, under Ar flow at a calcination of above 600 °C. In supported nano-Fe<sup>0</sup>, nanoparticles are exposed on the surface of the supports. Another concern of nano-Fe<sup>0</sup> is the stability in air.<sup>23,30,34</sup> Encapsulation of nano-Fe<sup>0</sup> into porous carbon spheres was suggested to be a promising way for enhancement of transportation, suspension, and stability of nanoscaled ZVI without significantly sacrificing activity.<sup>19,35</sup>

In this paper, we report a synthesis of nanoscaled Fe<sup>0</sup> (ca. 10 nm) encapsulated in microscale carbon spheres (6–8 μm) via an in situ formation from a glucose-induced hydrocarbonization, followed by a self-reduction. For the first time, we have discovered the activation of PMS using nanoscaled ZVI for the oxidation of phenol solutions. Supported cobalt/PMS were extensively investigated in our previous studies,<sup>12,36–38</sup> while cobalt is recognized as a priority pollutant that may cause many health issues.<sup>11</sup> The proposed nano-ZVI/PMS system exhibits superiority in the prevention of metal leaching.

## 2. EXPERIMENTAL SECTION

**Fabrication of Nano- $\text{Fe}^0$ @Microcarbon Spheres.** The nano- $\text{Fe}^0$ @CS materials were prepared via a green chemistry route without using any toxic compounds. Scheme 1 shows the formation process of

**Scheme 1. Fabrication of Nano- $\text{Fe}^0$ @Microcarbon Spheres**



the material. In a typical synthesis, 7.24 g of D-glucose (99.5%, Sigma) and 4.62 g of iron(III) nitrate nonahydrate (98%, Sigma-Aldrich) were dissolved in 80 mL of ultrapure water, and the mixture was then stirred for 4 h. The mixed solution was then transferred into a Teflon-lined autoclave (120 mL) and treated in an oven at 180 °C for 18 h. After cooling to room temperature, the obtained black suspension was filtered and washed by ethanol/water for three cycles. The precipitate was dried in an oven at 80 °C, and the obtained sample was labeled as Fe<sup>x</sup>@CS-f. The dried sample was further annealed in N<sub>2</sub> atmosphere in a tubular furnace at 350, 550, or 750 °C for 2 h, and the samples were denoted as Fe<sup>x</sup>@CS-350, Fe<sup>0</sup>@CS-550, and Fe<sup>0</sup>@CS-750, respectively.

Unsupported nanoscaled Fe<sup>0</sup> particles were prepared by reduction of Fe<sub>3</sub>O<sub>4</sub> nanopowder (<50 nm, Aldrich) under 10% H<sub>2</sub> in Ar at 550 °C for 6 h. The obtained ZVI aggregated into 2–5 μm particles. The prepared sample was marked as HR-Fe<sup>0</sup>. A commercial iron powder (45–150 μm, Chem Supply), denoted as commercial Fe<sup>0</sup>, was used as a reference material. Iron oxide (Fe<sub>2</sub>O<sub>3</sub>) and cobalt oxide (Co<sub>3</sub>O<sub>4</sub>)

were obtained via the thermal decomposition of iron(III) nitrate and cobalt(II) nitrate, respectively.

**Materials Characterization.** The crystalline structure of samples was analyzed by powder X-ray diffraction (XRD) using a Bruker D8-Avance X-ray diffractometer with Cu K $\alpha$  radiation ( $\lambda = 1.5418 \text{ \AA}$ ). The iron content and thermal stability of Fe<sup>x</sup>@CS and reference materials were investigated using thermogravimetric analysis–differential scanning calorimetry (TGA-DSC) in argon or air on a Mettler-Toledo Star<sup>e</sup> system. Fourier transform infrared (FTIR) spectra were acquired from a Bruker instrument, using an ATR mode. Scanning electron microscopy (SEM), energy-dispersive spectroscopy (EDS), and iron elemental mapping, performed on a Zeiss Neon 40EsB FIBSEM, were used to evaluate the morphology, size, and texture information of the samples. Transmission electron microscopy (TEM) was applied, using a JEOL 2011 TEM instrument. The Brunauer–Emmett–Teller (BET) surface area and pore size distribution were evaluated by nitrogen sorption at –196 °C, using a Quantachrome Autosorb AS-1 system. The samples were evaporated under vacuum at 200 °C for 4 h prior to the adsorption measurements.

**Adsorption and Catalytic Oxidation.** Oxidation of phenol solutions using ZVI with sulfate radicals was performed in a 1-L double-jacket reactor. The reaction temperature was maintained at 30 °C, using recycling water driven by a pump. In a typical run, 0.1 g of material was added into 200 mL of 20 ppm phenol solution. After stirring for 10 min, 0.4 g of Oxone was added into the mixed solution to start the reaction. At a set time interval, 1 mL of solution was withdrawn by a syringe and filtered through a Millipore film. The filtered solution was then injected into a vial, which was filled with 0.5 mL of methanol as a quenching reagent. Unsupported ZVI reaction was performed using an equivalent iron loading in Fe<sup>0</sup>@CS-550 at 0.115 g/L. Homogeneous iron/PMS system for phenol degradation was carried out using Fe(II) or Fe(III) ion solutions. In recycled experiments, used catalyst was collected by filtration, washed by water, and dried at 80 °C in air for reuse.

Adsorption experiments were carried out in a manner similar to the oxidation reactions, without the addition of oxidants and a quenching reagent.

The concentration of phenol solution was analyzed by high-performance liquid chromatography (HPLC, Varian) with a UV detector set at  $\lambda = 270 \text{ nm}$ . A C-18 column was used to separate the organics while the mobile phase, with a flow rate of 1.0 mL/min, was composed of 20% CH<sub>3</sub>CN and 80% water.

## 3. RESULTS AND DISCUSSION

**Characterization of Nano- $\text{Fe}^0$ @CS.** Figure 1 shows X-ray diffraction (XRD) patterns of three different samples containing zerovalent iron, nano-Fe<sup>0</sup>@CS-550, HR-Fe<sup>0</sup>, and commercial Fe<sup>0</sup> particles. The latter two samples showed a pure α-Fe with a body-centered cubic (bcc) crystalline structure, with Fe(110) at  $2\theta = 44.7^\circ$  and Fe(200) at  $2\theta = 64.9^\circ$ . No

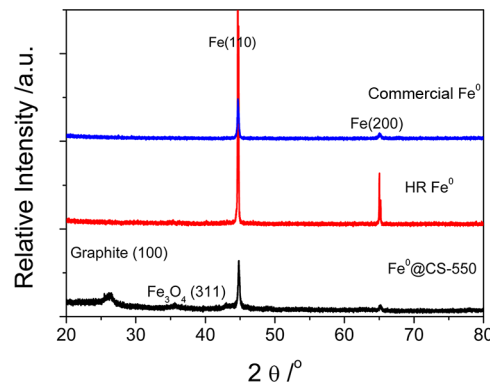


**Figure 1.** XRD patterns of nano Fe<sup>0</sup>@CS-550, HR Fe<sup>0</sup>, and commercial Fe<sup>0</sup>.

peaks assigned to iron oxides were observed.<sup>39</sup> The intensities of the peaks on HR-Fe<sup>0</sup> were much stronger than those of commercial Fe<sup>0</sup> particles. In the pattern of nano-Fe<sup>0</sup>@CS-550, besides the peaks of Fe<sup>0</sup>, a peak at 26.3° was observed, which was due to the (100) face of graphitic carbon.<sup>30</sup> Another weak peak at 35.6° was possibly due to the (311) face of Fe<sub>3</sub>O<sub>4</sub>.<sup>39</sup> XRD patterns of Fe<sup>x</sup>@CS-f and Fe<sup>x</sup>@CS-350 (see Figure S1 in the Supporting Information) did not have peaks that could be assigned to ZVI.

Figure 2 displays TGA profiles of Fe<sup>x</sup>@CS-f and ZVI samples in Ar or air. Figure 2A shows the phase transformation of iron

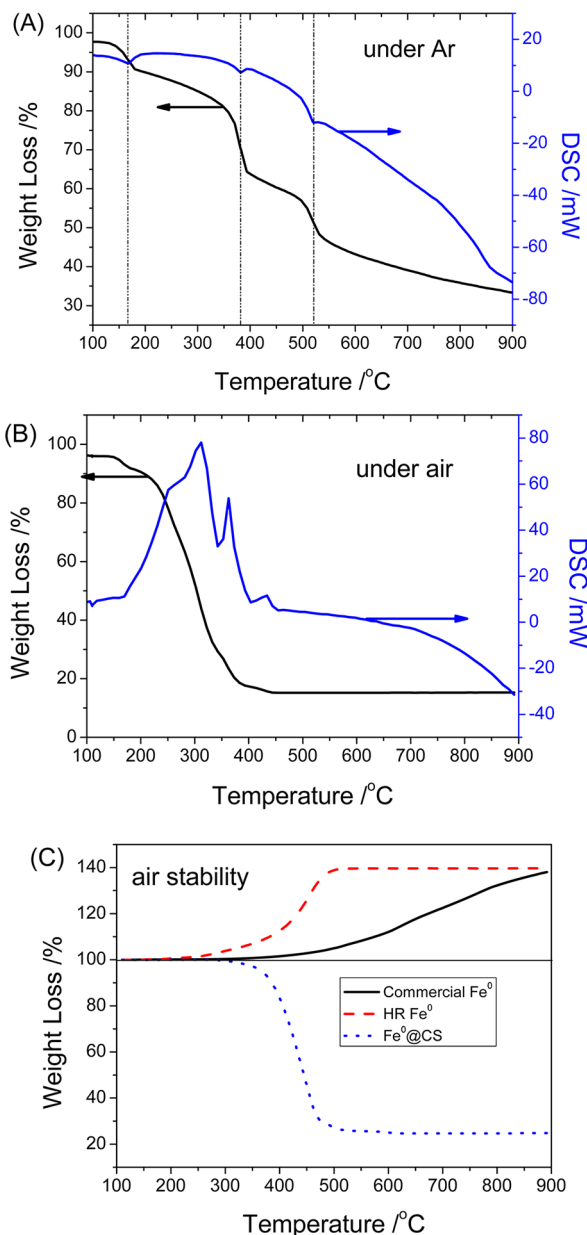


**Figure 2.** TGA profiles of Fe<sup>x</sup>@CS-f under (A) argon and (B) air, and (C) TGA comparison of three ZVI samples under air.

species and the desorption performance, under an argon atmosphere, of the fresh sample of Fe<sup>x</sup>@CS-f. Below 100 °C, only adsorbed water or ethanol was removed. Above 100 °C, three endothermic peaks were observed, at 167, 381, and 521 °C, respectively. The first peak arose from the transformation

of amorphous Fe(OH)<sub>3</sub> to FeOOH,<sup>40</sup> which was also indicated by XRD results. Fe<sup>x</sup>@CS-f and Fe<sup>x</sup>@CS-350 did not show any iron (oxide) peaks. The second endothermic peak at 381 °C was attributed to the transformation of FeOOH (or Fe<sub>2</sub>O<sub>3</sub>) to Fe<sub>3</sub>O<sub>4</sub>, and the peak at 521 °C was from the reduction of Fe<sub>3</sub>O<sub>4</sub> to Fe<sup>0</sup>.<sup>41</sup> Figure 2B shows the combustion performance of Fe<sup>x</sup>@CS-f. Exothermic peaks from 200 °C to 450 °C were from the decomposition and combustion of organics and amorphous carbon. Weight loss was determined to be stabilized at 15.0% after 444 °C, indicating the complete combustion of carbon and oxidation of iron with a final product of Fe<sub>2</sub>O<sub>3</sub>. The elemental iron loading on Fe<sup>x</sup>@CS-f was then calculated to be 10.5%. The elemental iron loadings in Fe<sup>x</sup>@CS-350, Fe<sup>0</sup>@CS-550, and Fe<sup>0</sup>@CS-750 were determined based on their TGA profiles (see Figure S2 in the Supporting Information) to be 14.2%, 22.9%, and 28.6%, respectively.

Figure 2C shows the weight changes of commercial Fe<sup>0</sup> powders, HR-Fe<sup>0</sup>, and nano-Fe<sup>0</sup>@CS-550. Weight increases of the first two samples were observed, indicating the oxidation of ZVI to iron oxides. Weight increase on commercial Fe<sup>0</sup> started at 284.9 °C, while it started at 181.4 °C on HR-Fe<sup>0</sup>. It suggested that the smaller size of ZVI is more easily oxidized in air. It was interesting to see that the weight remained unchanged on Fe<sup>0</sup>@CS until the temperature reached 296.2 °C, suggesting a better stability of Fe<sup>0</sup> on Fe<sup>0</sup>@CS.

Figure 3 shows FTIR spectra of prepared iron@CS samples annealed at different temperatures. The fresh sample of Fe<sup>x</sup>@

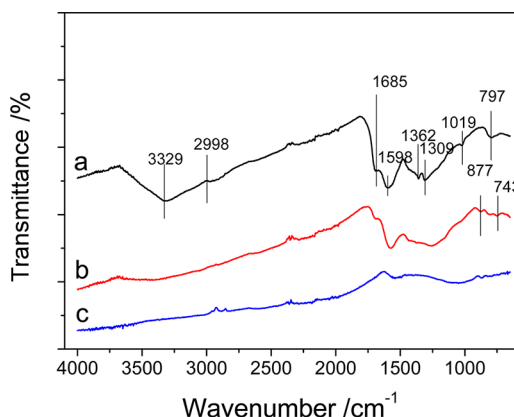


**Figure 3.** Fourier transform infrared (FTIR) spectra of Fe<sup>x</sup>@CS-f (spectrum a), Fe<sup>x</sup>@CS-350 (spectrum b), and Fe<sup>0</sup>@CS-550 (spectrum c).

CS-f without calcination presented many organic functional groups. The band at 1685 cm<sup>-1</sup> was attributed to C=O vibrations, and the peak of 1598 cm<sup>-1</sup> was assigned to C=C vibrations. The band at 1019 cm<sup>-1</sup> possibly arose from C–O stretching vibration, 1309 cm<sup>-1</sup> was from O–H bonding vibration, and 1360 cm<sup>-1</sup> indicated the presence of O–C=O. The band at 797 cm<sup>-1</sup> was due to aromatic C–H out-of-plane bending vibrations, while the band at 2998 cm<sup>-1</sup> was from stretching vibrations of aliphatic C–H. The band at 3329 corresponded to stretching vibrations of O–H. The results suggested that dehydration and aromatization occurred during the hydrothermal carbonization of glucose.<sup>42</sup> Calcination at 350 °C significantly reduced the intensities of the bands, indicating a further carbonization of the carbon spheres under N<sub>2</sub> atmosphere. In the spectrum of Fe<sup>x</sup>@CS-350, two new bands at 877 and 743 cm<sup>-1</sup> were observed, indicating the formation of

FeOOH.<sup>43</sup> Calcination at 550 °C under N<sub>2</sub> would remove most of the organic groups, while the band at 1598 cm<sup>-1</sup> assigned to C=C vibrations was still clear.

Figure 4 shows SEM images of Fe<sup>x</sup>@CS-f, Fe<sup>x</sup>@CS-350, Fe<sup>0</sup>@CS-550, and Fe<sup>0</sup>@CS-750. It was found that the prepared

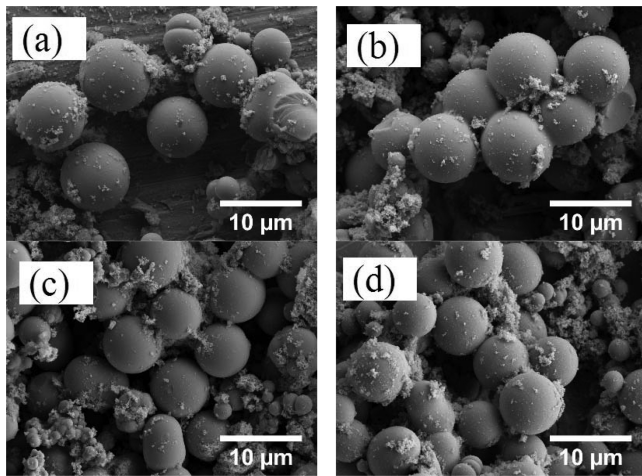


**Figure 4.** Scanning electron microscopy (SEM) images of (a) Fe<sup>x</sup>@CS-f, (b) Fe<sup>x</sup>@CS-350, (c) Fe<sup>0</sup>@CS-550, and (d) Fe<sup>0</sup>@CS-750.

iron–carbon composites showed a typical microspherical morphology. It is noted that the size of the carbon sphere is dramatically dependent on the synthesis conditions, such as glucose concentration, temperature and hydrothermal time.<sup>42</sup> In our study, a certain glucose concentration and hydrothermal condition were applied, and uniform carbon nanospheres can be obtained at the nanoscale level (see Figure S3 in the Supporting Information). The addition of an iron precursor significantly increased the size of carbon spheres, compared to bare spheres.

As a catalyst, microscale particles would be beneficial to easy separation. In this study, the size of the carbon sphere was ~6–8 μm. Besides the microspheres, some fine particles (50–200 nm) were found to attach to large spheres. Similar observation was reported by Yu et al.<sup>44</sup> In their study, Fe<sub>x</sub>O<sub>y</sub> was encapsulated in carbon spheres ca. 6 μm in size. Individual energy-dispersive X-ray spectroscopy (EDS) analysis focusing on large spheres (0.23 at.% Fe) and fine particles (0.32 at.% Fe) (see Figures S4 and S5 in the Supporting Information) showed similar iron atomic contents in Fe<sup>0</sup>@CS-550. The detected Fe loading was much lower than that from TGA, indicating that iron was encapsulated into carbon. It was also found that calcination did not influence the spherical morphology. However, high-resolution SEM (Figure S6 in the Supporting Information) focusing on the surface of spheres showed that a porous structure was developed during calcination.

Figure 5 shows TEM images of Fe<sup>x</sup>@CS-f and Fe<sup>0</sup>@CS-550. For analysis, the samples were thoroughly ground to crush the large spheres into fine particles (Figure S7 in the Supporting Information). It was seen that the large carbon spheres were aggregated by many nanoscale carbon particles (50–200 nm). The nanoscale carbon showed a core/shell-like structure, in which the core of ZVI was ~5–10 nm in diameter. Therefore, the nanoscale ZVI was evenly distributed and encapsulated by the spherelike carbon. The size of ZVI supported by polystyrene resins was found to be 5–20 nm, whereas Fe loadings were 4–14.5 wt %.<sup>25</sup> The size of ZVI supported by

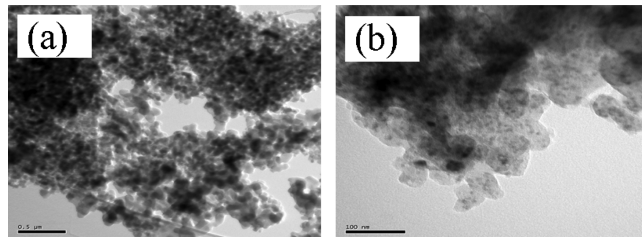


**Figure 5.** TEM images of (a) Fe<sup>x</sup>@CS-f and (b) Fe<sup>0</sup>@CS-550.

kaolinite was characterized to be 44.3 nm at a Fe loading of 20 wt %.<sup>28</sup> In NaY zeolite supported ZVI, the size was determined to be 50–100 nm at a Fe loading of 1.8 wt %.<sup>29</sup> In ZVI supported by activated carbon, at a Fe loading of 8.2 wt %, the iron particles showed a needlelike morphology, with dimensions of 30–500 nm × 1000–2000 nm.<sup>31</sup> It was recalled that, in this study, the Fe loading was 22.9 wt % in Fe<sup>0</sup>@CS-550. At such a high Fe content, Fe<sup>0</sup> was still confined to be a very tiny size (5–10 nm). Compared to other supported ZVI, which was distributed at the surface of supports, the formation of smaller-sized Fe<sup>0</sup> in our samples was attributed to the three-dimensional (3D) distribution of in-situ-formed carbon spheres. In the hydrothermal carbonization processes, a great variety of glucose reactions would take place and result in a complex mixture of organic compounds. At an increasing temperature, some aromatic compounds and oligosaccharides would form and then lead to a short single burst of nucleation. The nuclei then grew up uniformly and isotropically by diffusion of solutes toward the particle surfaces.<sup>42,45</sup> Once iron nitrate was introduced, the nuclei of Fe<sub>x</sub>O<sub>y</sub> would first appear. Then, Fe<sub>x</sub>O<sub>y</sub> would act as the nuclei for the subsequent formation of carbon spheres, because of the Coulombic interaction with the surface functional groups on carbon colloids. The produced Fe<sub>x</sub>O<sub>y</sub>-in-C nanorods would then be self-assembled to Fe<sub>x</sub>O<sub>y</sub>@C spheres via further intermolecular dehydration.<sup>35</sup> Therefore, large spheres and a homogeneous distribution of iron were fabricated.<sup>44</sup>

Figure 6 shows N<sub>2</sub> adsorption/desorption isotherms of Fe<sup>x</sup>@CS-f and Fe<sup>0</sup>@CS-550 and pore size distributions. The specific surface area ( $S_{\text{BET}}$ ) of Fe<sup>x</sup>@CS-f was calculated to be 24.1 m<sup>2</sup>/g. After calcination at 550 °C, the  $S_{\text{BET}}$  value of Fe<sup>0</sup>@CS-550 was significantly enhanced to be 414.4 m<sup>2</sup>/g. The specific surface area was higher than that of ZVI supported by carbon black (130 m<sup>2</sup>/g),<sup>30</sup> and also higher than another ZVI supported by carbon spheres (221 m<sup>2</sup>/g), which was activated at 1000 °C.<sup>33</sup> Referring to the International Union of Pure Applied Chemistry (IUPAC) classification, the adsorption isotherms of the samples were type IV and exhibited a type H2 hysteresis loop. A hysteresis loop at  $p/p_0 = 0.4$ –0.9 was observed on Fe<sup>0</sup>@CS-550, indicating the presence of a mesoporous structure.<sup>46,47</sup> The pore volumes of Fe<sup>x</sup>@CS-f and Fe<sup>0</sup>@CS-550 were 0.040 and 0.284 cm<sup>3</sup>/g, respectively. The size of their pores was similar centered at 6–7 nm. The increased pore volume and BET surface area after calcination were ascribed to the desorption of organic substances and partial oxidation of carbon by Fe<sub>x</sub>O<sub>y</sub>. The calcination would first desorb organic compounds and surface groups from the *in situ* formation of carbon spheres. Higher temperature led to the reduction reactions of Fe<sub>x</sub>O<sub>y</sub> and carbon around iron oxide was oxidized to CO<sub>2</sub>. Such reactions might act as activation processes for producing mesoporous pores in the carbon spheres. As

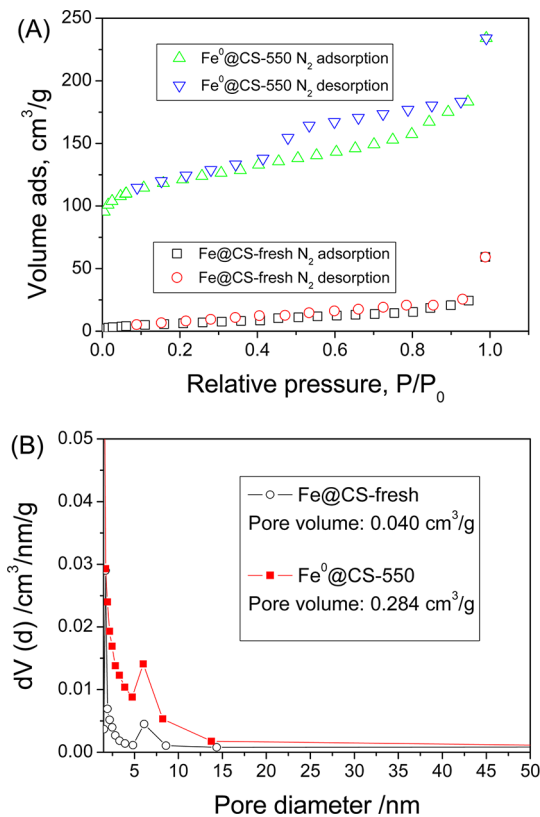


**Figure 6.** (A)  $N_2$  adsorption/desorption isotherms of  $Fe^x@CS-f$  and  $Fe^x@CS-550$  and (B) their pore size distributions.

previously mentioned, Figure S6 in the Supporting Information confirms the formation of porous structures after calcination.

#### Adsorption and Activation Performance of Nano- $Fe^0@CS$ .

Figure 7 shows the adsorption performances of iron

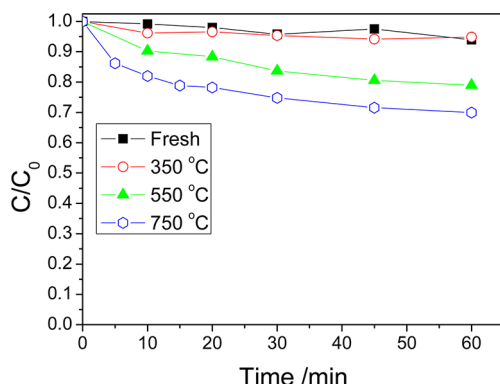


**Figure 7.** Adsorption of phenol on iron@CS at different calcination temperatures. [Conditions: phenol amount, 20 ppm; temperature, 30 °C; catalyst flow rate, 0.5 g/L.]

(oxide) $@CS$ , acquired from same procedure to oxidation without the addition of Oxone. The samples of  $Fe^x@CS-f$  and  $Fe^x@CS-350$  only presented a minor adsorption of phenol, giving 6% of phenol adsorption at 20 ppm in 60 min. The low adsorption was due to the small  $S_{BET}$  value and pore volume. Calcination under  $N_2$  would lead to further carbonization of the carbon spheres and desorption of the organic species, thereby resulted in a larger specific surface area. The reduction between iron oxide and carbon for the formation of ZVI would also

enlarge the pore volume of the carbon spheres. As a result,  $Fe^0@CS-550$  showed a phenol adsorption of 21%, while  $Fe^0@CS-750$  gave 30% phenol adsorption under the same conditions.

Figure 8 shows the oxidation of phenol solutions using iron/carbon annealed at different temperatures.  $Fe^x@CS-f$  was able

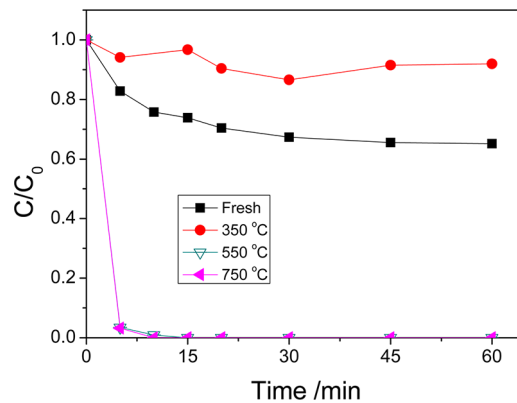


**Figure 8.** Effect of calcination temperature on the activity of oxidation of phenol with PMS. [Conditions: phenol amount, 20 ppm; temperature, 30 °C; PMS flow rate, 2 g/L; catalyst flow rate, 0.5 g/L.]

to degrade 34.8% of phenol at 60 min, while  $Fe^x@CS-350$  only removed 8.1% of phenol at the same time. As shown by TGA, the iron species in  $Fe^x@CS-f$  was iron(III) hydroxide, then the phenol oxidation was possibly due to the activation of PMS by Fe(III). Calcination at 350 °C might convert iron(III) hydroxide to be  $FeOOH$  or  $Fe_2O_3$ , resulting in a lower degradation rate. When the calcination temperature reached 520 °C or above, iron oxides would be reduced by carbon to ZVI. Therefore,  $Fe^0@CS-550$  and  $Fe^0@CS-750$  showed similar activity in the degradation of phenol with PMS. Both samples were able to completely decompose phenol in 15 min.

Figure 9 shows the performance of different ZVI materials in the activation of PMS for phenol degradation. Without a ZVI material, PMS was not able to degrade phenol by itself. At 90 min, the degradation efficiencies on commercial  $Fe^0$ , HR- $Fe^0$ , and  $Fe^0@CS-550$  were 15.8%, 54.6%, and 86.9%, respectively. The results strongly suggested that nanoscale ZVI can provide a

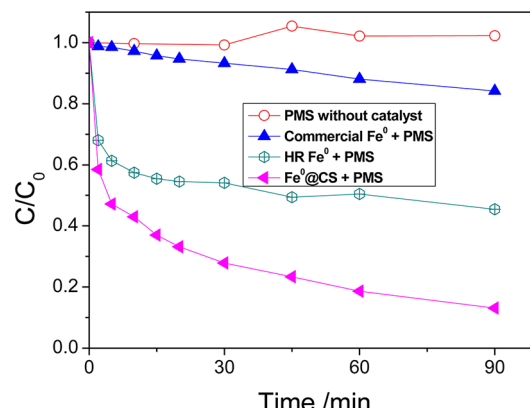


**Figure 9.** Degradation of phenol using different ZVI materials with PMS. [Conditions: phenol amount, 20 ppm; temperature, 25 °C; PMS flow rate, 0.5 g/L; catalyst flow rates, 0.5 g/L of  $Fe^0@CS-550$ , and 0.115 g/L of HR- $Fe^0$  and commercial  $Fe^0$ .]

faster activity in the oxidation of phenol: the smaller the size, the better the activity.

Figure 10 further compares the activities of various materials in homogeneous or heterogeneous activation of PMS for the

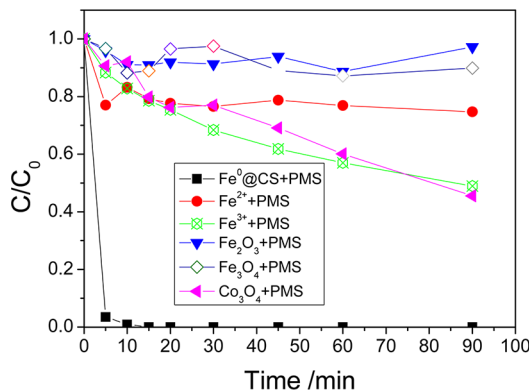


**Figure 10.** Degradation of phenol solutions using various catalysts. [Conditions: phenol amount, 20 ppm; temperature, 30 °C; PMS flow rate, 2 g/L; catalyst flow rates, 0.5 g/L of Fe<sup>0</sup>@CS-550, Fe<sub>2</sub>O<sub>3</sub>, Fe<sub>3</sub>O<sub>4</sub>, and Co<sub>3</sub>O<sub>4</sub>, and 0.05 M of Fe(II) and Fe(III).]

oxidation of phenol. It was seen that iron oxides (Fe<sub>2</sub>O<sub>3</sub> or Fe<sub>3</sub>O<sub>4</sub>) could only show minor activity, providing a phenol conversion of <10% after 90 min of reaction. In homogeneous reaction, Fe(II) showed 25.3% phenol degradation after 90 min, while Fe(III) produced 51.1% phenol degradation.

Cobalt oxide (Co<sub>3</sub>O<sub>4</sub>) has been widely used to activate PMS, and, so far, it has shown the best activity.<sup>11,12,37,48</sup> In this study, Co<sub>3</sub>O<sub>4</sub> that was prepared via the thermal decomposition of cobalt(II) nitrate was also tested and it produced 54.5% phenol removal after 90 min, which was comparable to that of Fe(III). Among all the materials, Fe<sup>0</sup>@CS-550 displayed the best performance in the activation of PMS for phenol degradation. It achieved complete phenol removal within 15 min.

In the reaction of HR-Fe<sup>0</sup> with PMS, it was found that Fe powders were completely dissolved during the reaction. It was interesting to evaluate the reusability of Fe<sup>0</sup>@CS-550 as well as its stability. It was found that the activity rapidly decreased after second and third runs, providing 31.7% and 13.4% phenol removal, respectively (see Figure S8 in the Supporting Information). The reduction in phenol degradation was possibly due to Fe<sup>0</sup> conversion to Fe(II)/Fe(III) in reaction. The corrosion processes led to decreased amounts of effective catalyst in the recovered material. Without the support of carbon spheres, the efficiency after the second run would be zero, because all of the ZVI was dissolved. Therefore, Fe<sup>0</sup>@CS-550 showed a better performance in reusability for potential application than bare ZVI, because of the remaining activity after second and third runs. Moreover, after the first run, the collected reaction solution was fed with phenol and PMS again at the same concentrations as in the first run, but it only showed 2% phenol removal, suggesting that dissolved Fe ions were ineffective for phenol oxidation.

The high activity and the stability of nano-Fe<sup>0</sup>@CS in the activation of PMS were due to the nature of ZVI and the unique structure. ZVI may provide a higher efficiency in activating PMS than Fe(II), as shown in eq 9:



In this case, the concentration of sulfate radicals produced by ZVI are 3 times higher than that of Fe(II) per mole. This is the reason why ZVI shows a higher activity than Fe ions and oxides. The mechanism of higher activity of nano-Fe<sup>0</sup>@CS than unsupported ZVI would be ascribed to the porous structure of carbon spheres and the core/shell structure of Fe@carbon. First, the encapsulation of carbon would play a significant role in the controllable release of Fe(II) ions. Second, the porous structure and the large S<sub>BET</sub> value would attract phenol molecules from the homogeneous solution to the surface of carbon spheres. Therefore, the SO<sub>4</sub><sup>2-</sup> produced would prefer to oxidize phenol, rather than be quenched by Fe(II). The carbon shell would also prevent the fast corrosion of iron as bare nano ZVI.

## 4. CONCLUSION

Nanoscaled zerovalent iron (ZVI) encapsulated in carbon spheres (nano-Fe<sup>0</sup>@CS) was fabricated using a green chemistry route. The structure of Fe<sup>0</sup>@CS consisted of carbon spheres (6–8 μm) composed of fine carbon particles (50–200 nm) encapsulating nanosized ZVI (5–10 nm). The iron/carbon hybrids annealed at 550 °C showed a porous structure with high specific surface area and pore volume. The carbon facilitated a good Fe dispersion by an in situ reduction and increased the stability of nanoscaled ZVI. Fe<sup>0</sup>@CS showed an efficient activity in producing oxidative radicals from PMS, thus leading to a superior performance in degradation of phenol to homogeneous iron/PMS and cobalt oxide/PMS. The higher activity of Fe<sup>0</sup>@CS was attributed to the nature of ZVI and the unique structure. The core of the design was to fabricate a porous structure for attracting substrates, and to controllably release Fe ions to avoid the quenching of active radicals. Therefore, nano-Fe<sup>0</sup>@CS-550 has been demonstrated to be a promising material for environmental remediation.

## ■ ASSOCIATED CONTENT

### S Supporting Information

XRD, TGA, SEM images, EDS, and reusability tests. This information is available free of charge via the Internet at <http://pubs.acs.org/>.

## ■ AUTHOR INFORMATION

### Corresponding Author

\*E-mail: Shaobin.wang@curtin.edu.au (S.W.), h.sun@curtin.edu.au (H.S.).

### Notes

The authors declare no competing financial interest.

## ■ REFERENCES

- Ryu, A.; Jeong, S. W.; Jang, A.; Choi, H. *Appl. Catal., B* **2011**, *105*, 128–135.
- Shi, Z. Q.; Nurmi, J. T.; Tratnyek, P. G. *Environ. Sci. Technol.* **2011**, *45*, 1586–1592.
- Zhang, M.; He, F.; Zhao, D. Y.; Hao, X. D. *Water Res.* **2011**, *45*, 2401–2414.
- Song, H.; Caraway, E. R. *Environ. Sci. Technol.* **2005**, *39*, 6237–6245.
- Bandstra, J. Z.; Miehr, R.; Johnson, R. L.; Tratnyek, P. G. *Environ. Sci. Technol.* **2005**, *39*, 230–238.
- Nam, S.; Tratnyek, P. G. *Water Res.* **2000**, *34*, 1837–1845.
- Keum, Y. S.; Li, Q. X. *Chemosphere* **2004**, *54*, 255–263.
- Ponder, S. M.; Darab, J. G.; Mallouk, T. E. *Environ. Sci. Technol.* **2000**, *34*, 2564–2569.

- (9) Yoon, I. H.; Kim, K. W.; Bang, S.; Kim, M. G. *Appl. Catal., B* **2011**, *104*, 185–192.
- (10) Joo, S. H.; Feitz, A. J.; Waite, T. D. *Environ. Sci. Technol.* **2004**, *38*, 2242–2247.
- (11) Shukla, P.; Sun, H. Q.; Wang, S. B.; Ang, H. M.; Tade, M. O. *Catal. Today* **2011**, *175*, 380–385.
- (12) Shukla, P. R.; Wang, S. B.; Sun, H. Q.; Ang, H. M.; Tade, M. O. *Appl. Catal., B* **2010**, *100*, 529–534.
- (13) Kim, D. H.; Kim, J.; Choi, W. *J. Hazard. Mater.* **2011**, *192*, 928–931.
- (14) Lee, C.; Keenan, C. R.; Sedlak, D. L. *Environ. Sci. Technol.* **2008**, *42*, 4921–4926.
- (15) Kallel, M.; Belaid, C.; Boussahel, R.; Ksibi, M.; Montiel, A.; Elleuch, B. *J. Hazard. Mater.* **2009**, *163*, 550–554.
- (16) Zhou, T.; Li, Y. Z.; Ji, J.; Wong, F. S.; Lu, X. H. *Sep. Purif. Technol.* **2008**, *62*, 551–558.
- (17) Boussahel, R.; Harik, D.; Mammar, M.; Lamara-Mohamedl, S. *Desalination* **2007**, *206*, 369–372.
- (18) Kusic, H.; Peternel, I.; Ukić, S.; Koprivanac, N.; Bolanca, T.; Papic, S.; Bozic, A. L. *Chem. Eng. J.* **2011**, *172*, 109–121.
- (19) Zhao, J. Y.; Zhang, Y. B.; Quan, X.; Chen, S. *Sep. Purif. Technol.* **2010**, *71*, 302–307.
- (20) Liang, C. J.; Guo, Y. Y. *Environ. Sci. Technol.* **2010**, *44*, 8203–8208.
- (21) Lee, Y. C.; Lo, S. L.; Chiueh, P. T.; Liou, Y. H.; Chen, M. L. *Water Res.* **2010**, *44*, 886–892.
- (22) Liang, C. J.; Lai, M. C. *Environ. Eng. Sci.* **2008**, *25*, 1071–1077.
- (23) Rastogi, A.; Ai-Abed, S. R.; Dionysiou, D. D. *Appl. Catal., B* **2009**, *85*, 171–179.
- (24) Li, Y. M.; Zhang, Y.; Li, J. F.; Zheng, X. M. *Environ. Pollut.* **2011**, *159*, 3744–3749.
- (25) Jiang, Z. M.; Lv, L.; Zhang, W. M.; Du, Q. O.; Pan, B. C.; Yang, L.; Zhang, Q. X. *Water Res.* **2011**, *45*, 2191–2198.
- (26) Karabelli, D.; Unal, S.; Shahwan, T.; Eroglu, A. E. *Chem. Eng. J.* **2011**, *168*, 979–984.
- (27) Chen, Z. X.; Jin, X. Y.; Chen, Z. L.; Megharaj, M.; Naidu, R. J. *Colloid Interface Sci.* **2011**, *363*, 601–607.
- (28) Zhang, X.; Lin, S.; Chen, Z. L.; Megharaj, M.; Naidu, R. *Water Res.* **2011**, *45*, 3481–3488.
- (29) Wang, W.; Zhou, M. H.; Mao, Q. O.; Yue, J. J.; Wang, X. *Catal. Commun.* **2010**, *11*, 937–941.
- (30) Hoch, L. B.; Mack, E. J.; Hydutsky, B. W.; Hershman, J. M.; Skluzacek, I. M.; Mallouk, T. E. *Environ. Sci. Technol.* **2008**, *42*, 2600–2605.
- (31) Zhu, H. J.; Jia, Y. F.; Wu, X.; Wang, H. *J. Hazard. Mater.* **2009**, *172*, 1591–1596.
- (32) Lv, X. S.; Xu, J.; Jiang, G. M.; Xu, X. H. *Chemosphere* **2011**, *85*, 1204–1209.
- (33) Sunkara, B.; Zhan, J. J.; He, J. B.; McPherson, G. L.; Piringer, G.; John, V. T. *ACS Appl. Mater. Interfaces* **2010**, *2*, 2854–2862.
- (34) Sohn, K.; Kang, S. W.; Ahn, S.; Woo, M.; Yang, S. K. *Environ. Sci. Technol.* **2006**, *40*, 5514–5519.
- (35) Liu, H. B.; Xu, J. L.; Li, Y. J.; Li, Y. L. *Acc. Chem. Res.* **2010**, *43*, 1496–1508.
- (36) Shukla, P.; Sun, H. Q.; Wang, S. B.; Ang, H. M.; Tade, M. O. *Sep. Purif. Technol.* **2011**, *77*, 230–236.
- (37) Shukla, P.; Wang, S. B.; Singh, K.; Ang, H. M.; Tade, M. O. *Appl. Catal., B* **2010**, *99*, 163–169.
- (38) Shukla, P.; Wang, S. B.; Sun, H. Q.; Ang, H. M.; Tade, M. O. *Chem. Eng. J.* **2010**, *164*, 255–260.
- (39) Crane, R. A.; Dickinson, M.; Popescu, I. C.; Scott, T. B. *Water Res.* **2011**, *45*, 2931–2942.
- (40) Bumajdad, A.; Ali, S.; Mathew, A. *J. Colloid Interface Sci.* **2011**, *355*, 282–292.
- (41) Feyzi, M.; Irandoost, M.; Mirzaei, A. A. *Fuel Process. Technol.* **2011**, *92*, 1136–1143.
- (42) Sevilla, M.; Fuertes, A. B. *Chem.—Eur. J.* **2009**, *15*, 4195–4203.
- (43) Zhang, T.; Li, C. J.; Ma, J.; Tian, H.; Qiang, Z. M. *Appl. Catal., B* **2008**, *82*, 131–137.
- (44) Yu, G. B.; Sun, B.; Pei, Y.; Xie, S. H.; Yan, S. R.; Qiao, M. H.; Fan, K. N.; Zhang, X. X.; Zong, B. N. *J. Am. Chem. Soc.* **2010**, *132*, 935–936.
- (45) Sun, X. M.; Li, Y. D. *Angew. Chem., Int. Ed.* **2004**, *43*, 597–601.
- (46) Hardjono, Y.; Sun, H. Q.; Tian, H. Y.; Buckley, C. E.; Wang, S. B. *Chem. Eng. J.* **2011**, *174*, 376–382.
- (47) Zhou, G. L.; Tian, H. Y.; Sun, H. Q.; Wang, S. B.; Buckley, C. E. *Chem. Eng. J.* **2011**, *171*, 1399–1405.
- (48) Zhou, G. L.; Sun, H. Q.; Wang, S. B.; Ang, H. M.; Tade, M. O. *Sep. Purif. Technol.* **2011**, *80*, 626–634.